Письма в ЭЧАЯ. 2006. Т. 3, № 1(130). С. 31–44

УДК 539.1.074.59, 539.184.3

THERMAL SPIKE MODEL OF TRACK FORMATION IN $YBa_2Cu_3O_{7-x}$

B. F. Kostenko, J. Pribiš, I. N. Goncharov

Joint Institute for Nuclear Research, Dubna

We consider a model based on the thermal spike concept for an explanation of latent track formation in $YBa_2Cu_3O_{7-x}$ single crystal. The model demonstrates some interesting peculiarities such as «electronic quenching» and existence of bifurcation points. Arguments why the energy spent on damage creation in the track should be equal to melting heat and why the so-called «epitaxial regrowth» is impossible are given.

Для объяснения процессов формирования треков в монокристалле $YBa_2Cu_3O_{7-x}$ предложено описание, основанное на модели термического пика. Модель демонстрирует некоторые интересные особенности: явление «электронной закалки» и бифуркационную зависимость решения от параметров. Показано, что энергия, затраченная на создание трека, должна быть равна теплоте плавления, а также что модель «эпитаксиального восстановления» неприменима.

INTRODUCTION

With the miniaturization of technologies enabling nanodimensions ion track engineering takes now on special significance. Particularly, latent swift heavy ion tracks in high-T_c superconductors are able to act as vortex pinning centers and to increase dramatically the critical current density of the materials [1–3]. At present no satisfactory theory of track formation in high-T_c superconductors exists in spite of the manifest practical importance of this application. Theoretically, several different mechanisms, among which are the thermal spike [4], the ionic spike [5] or more refined models [6, 7], are possible for explanation of the process. The ionic spike model explains the track formation by creation of a positive ion cloud around the projectile path, which «explodes» due to electrostatic repulsion (Coulomb explosion). According to the thermal spike model, the material melts within a cylinder along the trajectory of an energetic ion if the temperature exceeds the melting point. Subsequent fast cooling down leads to amorphous phase formation in place of melted one, i.e., to latent track constitution.

The first attempt to develop a thermal spike model (TSM) to provide a theoretical description of track formation in high-T_c superconductors was undertaken in [8]. Physical reasons which led the authors to this suggestion have been the following: nanodiffraction from the region of tracks in $YBa_2Cu_3O_{7-x}$ shows that they are *amorphous*; transmission electron microscopy revealed lattice distortion corresponding to *dilation* of the material inside tracks [8, 9]. Although both of these facts can be interpreted as the result of melting (accompanied with expansion of the material) with subsequent its solidification, other explanations are possible too. Therefore, investigations with almost the same experimental technique led the authors of [2] to a conclusion that the mechanism of track formation in $YBa_2Cu_3O_{7-x}$ is based on the ionization process [5].

The first thermal spike description of track formation in high-T_c superconductors neglected latent heat of melting and, therefore, predicted track radii greater than experimental ones. To justify this difference, an interesting hypothesis of «epitaxial regrowth» was suggested according to which the molten region does not all become amorphous, but the outer part of it should undergo recrystallization. In such a way an attempt to gain a deep insight into the problem and go beyond the traditional thermal spike framework was also undertaken in [8], although it looks now slightly premature because of the above mentioned inaccuracy of the model.

In [10], a phenomenological approach based on the thermal spike concept was proposed to explain the evolution of track sizes with energy deposition for irradiated $YBa_2Cu_3O_{7-x}$ and $Bi_2Sr_2CaCu_2O_8$ superconductors. Although this model was successful in its design, it contained some parameters independent of the physical properties of the materials and could be only considered as a useful preliminary investigation of the problem.

A more detailed model of track formation in $YBa_2Cu_3O_{7-x}$ based on a system of coupled equations for electron and atom temperatures was proposed in [11] by analogy with a thermal spike model developed in Caen [12] for description of latent track formation in amorphous metals and semiconductors. The mean free path of electron scattering, $\lambda = \sqrt{D_e \tau}$, is assumed to be the only free parameter in this version of TSM. Here D_e is the diffusivity of the excited electrons in the vicinity of ion trajectory which is usually supposed to be a constant (for a given material) belonging to the range 1–2 cm^2/s [14]. Parameter τ is the electron–atom relaxation time approximately determined in femtosecond laser experiments [15, 16]. Other quantities used in the model are known macroscopic characteristics of an irradiated matter such as thermal conductivities of electrons and atoms, K_e and K_i, their specific heats, C_e and C_i, density ρ of solid and liquid phases, melting temperature T_m, and heat of fusion Q_f.

The value of parameter $\lambda \simeq 18$ nm found in [11] for $YBa_2Cu_3O_{7-x}$ was close to the corresponding magnitude obtained for amorphous metals and semiconductors, electron–atom relaxation time τ turned out to be in good agreement with femtosecond laser experiments, and all that seemed to be quite reasonable. However, simple analytical estimations fulfilled in [11] have shown that the experimentally observed dependence of track radii on energy deposition can be solely explained if one takes into account an approximate linear dependence of τ on T_e (such a dependence follows, in particular, from Allen's theory [17]). At this point the description of track formation in $YBa_2Cu_3O_{7-x}$ deviates from the Caen version of TSM where τ is usually supposed to be temperature-independent. In the present paper we take into account the $\tau(T_e)$ dependence by *explicit* substitution of the $\tau(T_e)$ function into the system of equations describing track formation. Besides, other basic assumptions of TSM are discussed in much more detail.

1. MAIN EQUATIONS AND BOUNDARY CONDITIONS

We assume the following system of two coupled nonlinear differential equations (see [12] and references therein):

$$\rho C_e(T_e)\frac{\partial T_e}{\partial t} = \frac{1}{r}\frac{\partial}{\partial r}\left[rK_e(T_e)\frac{\partial T_e}{\partial r}\right] - g(T_e - T_i) + q(r,t), \tag{1}$$

$$\rho C_i(T_i)\frac{\partial T_i}{\partial t} = \frac{1}{r}\frac{\partial}{\partial r}\left[rK_i(T_i)\frac{\partial T_i}{\partial r}\right] + g(T_e - T_i), \tag{2}$$

where T_e and T_i are electrons' and lattice temperatures, respectively; g is the electron–atom coupling; $q(r,t)$ the power brought on the electronic system; r the radius in cylindrical geometry with the ion path as the axis. The energy loss caused by direct ion-nuclear collisions, which can be estimated by the Rutherford formula, is two orders of magnitude less than the energy loss due to electronic excitations [13]. Ion energy loss transmitted into radiation is negligible too. Equations (1) and (2) disregard z-dependence of T_e and T_i since ion energy losses change rather slowly along z and stopping scale essentially exceeds the track radii. It is supposed in (1) that electrons receive their energy from the external source $q(r,t)$ which describes ion energy loss in electron gas. According to (2), atoms are heated due to electron–atom coupling represented by the term $g(T_e - T_i)$.

The initial conditions can be chosen in the form

$$T_e(r,0) = T_i(r,0) = T_0,$$

and the boundary ones can be taken as

$$\left(\frac{\partial T_e}{\partial r}\right)_{r=r_{\min}} \left(\frac{\partial T_i}{\partial r}\right)_{r=r_{\min}} = 0, \qquad T_e(r_{\max},t) = T_i(r_{\max},t) = T_0,$$

where T_0 is temperature of the environment and no-heat-transfer condition at the center of track $r = r_{\min}$ is taken into account. Parameter $r_{\min} = 0.1$ nm is introduced to avoid difficulties with description of energy deposition at point $r = 0$, and $r_{\max} = 10^{-5}$ cm is a physical infinity as used here.

2. MODEL OF ENERGY DEPOSITION

The radial distribution of dose around the path of a heavy ion can be calculated in line with the delta-ray model of track structure, which is widespread in radiation dosimetry [18]. The model incorporates energy deposition due to primary excitations and ionization of atoms, and δ-electron kinetic energy transfer. According to it, the primary excitations contribute essentially, about 50%, in the region $r < 10$ nm. For $r > 10$ nm investment of δ electrons entirely dominates. Energy expended on ionization is taken into account using some mean ionization potential, of about 10 eV, which is subtracted from δ-electron kinetic energy. The stopping power calculated as the radially integrated dose distribution is in agreement with SRIM code [21] predictions within 12%. Although such a precision reflects current ability of the theory, we renormalized the radial distribution of energy deposition [18] to the SRIM stopping power, often considered as a standard.

The radial distribution of dose cannot be regarded as instantaneous at least for $t \geqslant 10$ fs when the thermal diffusivity of excited electron, $D_e \sim 1$ cm^2/s, should be taken into account. Further development of the delta-ray model [18] in the required direction was undertaken in [19], where dissipation of the energy stored up in δ electrons was described. In the first approximation, the δ electrons' trajectories can be considered to be perpendicular to the ion one, so that the time of electron arrival to a point at a distance b from the center of ion path is equal to

$$t(b) = \int_0^b \frac{db}{v(b)} = \int_{R-b}^{R} \frac{dr}{v(R-r)} = \frac{1}{c}\int_{E(R-b)}^{E(R)} dE \left(\frac{dr}{dE}\right) \frac{E + mc^2}{[E(E+2mc^2)]^{1/2}}, \qquad (3)$$

$r = r(E)$ being the range-energy relation for electrons in the material; c is the speed of light; m is the electron mass. The energy deposition at moment t in volume $2\pi b db\times$ unit pathlength is determined by

$$\varepsilon(b,t) = \frac{1}{2\pi b}\int_{E(b,t)}^{E_{\max}} \left(-\frac{dE(R-b)}{db}\right)\frac{dN}{dE}dE,$$

where $E(b,t)$ is the solution of Eq. (3), dN/dE stands for the number of delta rays per energy unit which is calculated using the Rutherford formula. The range-energy relation $r(E)$ and its inverse $E(r)$ were approximated in [18] from known experimental and theoretical data. Thus, the space-time distribution of energy deposition, including its dependence on the projectile velocity, can be taken into account at least for $t > 10$ fs and $r > 10$ nm, when δ-electron kinetic energy contribution to energy deposition utterly prevails. This improvement of the TSM is important in view of an experiment [20], where the projectile velocity influence on track formation was reported.

For $t < 10$ fs the δ-electron dynamics, as the slowest one, can also be used to find the moment when the energy deposition is stopped at a given point. The most part of energy spent on track creation is released within the region $r < 1$ nm and $t < 0.15$ fs, although the process persists up to $t \sim 10^{-5}$ s and $r \sim 10^{-3}$ cm [19]. Calculations show that δ-electron energy deposition at $r < 10$ nm comes to the end by the time of $t \sim 10$ fs. On the other hand, just by this moment Auger decays of all vacancies in the electron shells are expected to occur and thermodynamic equilibrium for the excited electrons to be established. Therefore, exactly the moment $t \simeq 10$ fs should be considered as a proper initial time, when the basic equations of TSM, (1) and (2), may be used in a consistent manner with the radial distribution of dose at that moment estimated by the simple δ-electron dissipation dynamics.

An interesting attempt to examine experimentally the delta-ray model [18] and penetrate into region $t < 10$ fs, $r < 10$ nm was undertaken in [27] for tracks in amorphous carbon. Although a distinct difference was revealed (more higher electron temperatures in the valence band at $r < 1$ nm and more lower temperatures for $1 < r < 10$ nm), it looks like the experimental temperature probe is really taken a few earlier, at $t \sim 1$ fs, so that the prediction of the delta-ray model [18] should be in an acceptable agreement with those data by the moment $t \sim 10$ fs.

3. DESCRIPTION OF THE ELECTRONIC SUBSYSTEM

The basic equations (1) and (2) are nothing else but energy conservation laws which tolerate both quantum and classical physics specification implemented in thermal physics constants, particularly, in specific heat and thermal conductivity of electronic and atom subsystems. Thermal capacity of electrons in a wide temperature interval can be found numerically according to the formula (see, e.g., [22])

$$\rho C_e(T_e) = \int \varepsilon\, \frac{f(\varepsilon, T_e)}{dT_e}\, dn(\varepsilon),$$

where $f(\varepsilon, T_e)$ is the Fermi distribution; $dn(\varepsilon) = \eta(\varepsilon)d\varepsilon$, and $\eta(\varepsilon)$ is the electronic density of states given for $YBa_2Cu_3O_{7-x}$ in [23]. Calculated and an experimentally estimated value of Sommerfeld's parameter, $\gamma = \rho C_e/T_e$, is $(2.4 \pm 0.8)\cdot 10^{-4}$ J/(cm$^3\cdot$K^2) [24].

According to [25], the electronic thermal conductivity of $YBa_2Cu_3O_{7-x}$ equals to $K_e = 2.5 \cdot 10^{-2}$ W/(cm · K) in plane (001) at $T_e \simeq 300$ K. This, with taking into account the previous estimation for γ, corresponds to the value of electron diffusivity $D_e \equiv K_e/\rho C_e = 0.26 \div 0.52$ cm^2/s. At higher temperatures K_e and D_e are unknown yet. The choice $D_e = 1{-}2$ cm^2/s accepted in the Caen version of TSM is motivated by reasons that «hot electrons in the conduction band behave like in metals» and the value of this order is usually suggested for metals at high temperatures [26]. Since these arguments seem to be plausible at least at the qualitative description, the constant value $D_e = 2$ cm^2/s was assumed in [11]. More detailed consideration, however, predicts both temperature and material dependence of D_e. For example, using calculation performed for amorphous carbon in [27], one can found a monotonous growth of D_e for T_e change from $2 \cdot 10^3$ to $5 \cdot 10^4$ K. Furthermore, a dependence of D_e on T_e is expected to exist in general case from the obvious physical reasons like influence of electron temperature on electron–electron and electron–ion cross sections. Therefore, in this study we suppose D_e to be an adjusting parameter which should be determined from the requirement of correct description of measured track radii. However, it cannot be reputed as a true free parameter because its value is approximately assessed to be near to 1 cm^2/s in track formation processes.

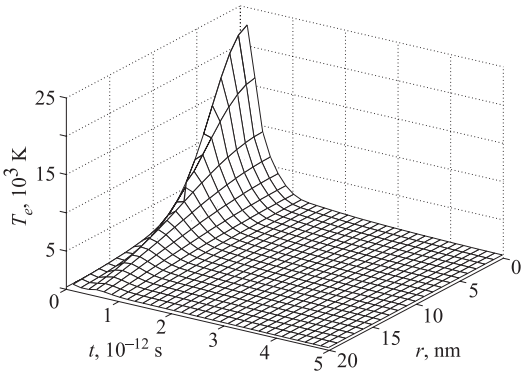

Fig. 1. $T_e(r,t)$ distribution for ion ^{129}Xe at 2.6 MeV/amu in $YBa_2Cu_3O_{7-x}$. At the moment of electron subsystem relaxation to the thermodynamic equilibrium, $t \simeq 10^{-15}$ s, the temperature of electrons in the center of track is about 10^5 K

Electron thermal conductivity in (1) can be expressed through D_e by the formula

$$K_e = D_e \rho C_e,$$

where, as was mentioned above,

$$\rho C_e = \gamma T_e, \quad \gamma \approx 2.4 \cdot 10^{-4} \text{ J}/(\text{cm}^3 \cdot \text{K}^2).$$

The effective electron–atom relaxation time, τ, can be naturally introduced after a brief examination of Eq. (1),

$$\tau = \rho C_e / g.$$

Due to linear dependence of C_e on T_e, function $\tau(T_e)$ acquires the same linear form, $\tau = (\gamma/g)\, T_e \equiv \alpha T_e$, as was predicted by Allen's theory [17], where

$$\tau = \frac{\pi}{3}\frac{k_B}{\lambda'\langle\omega^2\rangle}T_e.$$

Using the experimental value of $\lambda'\langle\omega^2\rangle(475 \pm 30)$ meV^2 established in [15], one can estimate parameter α from Allen's theory:

$$\alpha = (1.28 \pm 0.06) \cdot 10^{-16}\ \text{s/K}.$$

In such a way, electron–atom coupling g turns out to be expressed in Eq. (1) through α and γ parameters: $g = \gamma/\alpha$. In fact, the following form of Eq. (1) was found the most convenient for numerical solution:

$$\rho C_e(T_e)\frac{\partial T_e}{\partial t} = \frac{1}{r}\frac{\partial}{\partial r}\left[rD_e\rho C_e(T_e)\frac{\partial T_e}{\partial r}\right] - \frac{\rho C_e(T_e)}{\tau(T_e)}(T_e - T_i) + q(r,t). \tag{4}$$

Figure 1 shows a distribution of electron temperature $T_e(r,t)$ in the vicinity of ion ^{129}Xe at 2.6 MeV/amu in $YBa_2Cu_3O_{7-x}$. Although the distribution in Fig. 1 was found as a solution of coupled system (2) and (4) (with physical parameters defined later) for times $t \sim 10^{-13}$ s the inequality $T_e \gg T_i$ holds, so that the early stage of energy relaxation process is controlled by sole Eq. (4) in which one can omit T_i or substitute $T_i = T_0$.

4. DESCRIPTION OF THE ATOMIC SUBSYSTEM

Utilization of electrons' and atoms' temperatures, T_e and T_i, in the TSM should not conceal the fact that true thermodynamic equilibrium states, either liquid or solid, are not expected to form during the period of energy excitation in the track ($\Delta t \simeq 0.6 \cdot 10^{-11}$ s, see Fig. 6 below). Therefore, experimental values such as specific heat and heat of fusion, being measured at thermodynamic equilibrium, could not be formally accepted as the model parameters without special investigation of their nature. For example, the experiment shows that the temperature dependence of $YBa_2Cu_3O_{7-\delta}$ heat capacity contains several high peaks in the range from 300 to 800 °C with total contribution to the absorbent heat of about 62–65 J/g [28]. However, since this contribution is mainly caused by rather slow thermal desorption of oxygen from the material (see [28]), we did not take it into account. Description of melting comprises a similar problem. Here one has to keep in mind that melting point, apart from the fact that it marks the temperature at which liquid and solid phases coexist in thermodynamic equilibrium, indicates in more general sense the location of a structural instability of matter upon further heating or cooling. Distinguishing between these two aspects is especially important for any nonequilibrium system, similar to the one considered in this paper, where the ergodicity hypothesis is inapplicable (see, e.g., [29]).

The melting temperature T_m of $YBa_2Cu_3O_{7-\delta}$ found by real time neutron diffraction analysis is nearly 1070 °C [30]. If this temperature is held long enough, the peritectic reaction $\alpha + L \rightarrow \beta$ will occur, where α is the high-temperature solid phase, L is the liquid phase,

β is the low-temperature solid phase. When $YBa_2Cu_3O_{7-\delta}$ is heated above, it incongruently melts according to the reactions [31]

$$YBa_2Cu_3O_7 \rightarrow Y_2BaCuO_5 + \text{liquid}, \quad T < 1300\,^\circ\text{C},$$

$$Y_2BaCuO_5 + \text{liquid} \rightarrow Y_2O_3 + \text{liquid}, \quad 1300 < T < 1500\,^\circ\text{C}.$$

Although the calculations show that the lattice temperature in the vicinity of ion's trajectory can exceed the melting temperature, it would be unrealistic suggesting any chemical reactions to take place during a picosecond time interval. Therefore, it is natural to put also on trial one of the main suggestion of TSM that energy expended on the amorphous track formation, Q_a, coincides with the heat Q_m necessary for melting of the lattice inside the track. In the presented calculations we accept the traditional TSM estimation, $Q_a = Q_m$, which seems to be true at least approximately (see discussion below). The value of Q_m follows from paper [32], where an oxygen pressure dependence of melting point in the reaction

$$YBa_2Cu_3O_{7-\delta} \rightarrow \text{solid} + \text{liquid} + O_2$$

was investigated. The usual consideration based on Clapeyron–Clausius equation allows one to find the enthalpy change of the reaction, $Q_m = (810 \pm 5)$ kJ/mol. In fact, such an estimation is perhaps somewhat inaccurate because it sums up a contribution of the endothermic reaction of oxygen desorption.

For lattice thermal capacity, the Dulong–Petit value, $\rho C_i = 3.1\ \text{J} \cdot \text{cm}^{-3} \cdot \text{K}^{-1}$, was taken, where $\rho = 6.39\ \text{g} \cdot \text{cm}^{-3}$. Thermal conductivity of atomic system, K_i, was chosen in accordance with [17, 25, 33, 34], $K_i = 5.6 \cdot 10^{-2}\ \text{J} \cdot (\text{s} \cdot \text{cm} \cdot \text{K})^{-1}$. Since K_i is suggested to be temperature-independent, thermal diffusivity $D_i = K_i/\rho C_i$ can be introduced, and Eq. (2) can be replaced by

$$\frac{\partial T_i}{\partial t} = D_i^{\text{eff}}(T_i) \triangle T_i + \frac{1}{\tau(T_e)} \frac{C_e(T_e)}{C_i^{\text{eff}}(T_i)} (T_e - T_i), \tag{5}$$

with functions $\tau(T_e)$, $C_e(T_e)$ defined in the previous section and

$$C_i^{\text{eff}} = C_i + Q_m\ \delta(T_m - T_i) \tag{6}$$

being the effective specific heat which includes the melting heat, $Q_m = 1.216$ kJ/g. Formally, one has to put in (5)

$$D_i^{\text{eff}}(T_i \neq T_m) = D_i,$$

and

$$D_i^{\text{eff}}(T_i = T_m) = 0$$

due to δ-function presence in the denominator of the expression for D_i.

To solve numerically the system (4) and (5), a *regularization* of C_i^{eff} and $D_i^{\text{eff}} = K_i/\rho C_i^{\text{eff}}$ was performed in neighborhood $T_m - \Delta \leqslant T_i \leqslant T_m + \Delta$ of melting temperature:

$$C_i^{\text{eff}}(T_i) = C_i + \frac{Q_f - 2C_i\Delta}{\sigma\sqrt{2\pi}} \exp\left(-\frac{(T_i - T_m)^2}{2\sigma^2}\right). \tag{7}$$

Parameters σ and Δ were chosen as follows: $\sigma = 5$ K, $\Delta = 4.5\ \sigma$.

5. PECULIARITIES OF SOLUTION

The numerical solution of system (4), (5) is based on finite-difference scheme due to Samarskii [40], for differential heat equations (see [41]).

Numerically found solutions of the system with parameters corresponding to $YBa_2Cu_3O_{7-x}$ demonstrate some interesting and unexpected features. The first of them is caused by the presence of the power deposition term $q(x,t)$ in the starting equations. In Fig. 2 temperature distribution $T_i(r,t)$ for ion ^{129}Xe at 2.6 MeV/amu is depicted.

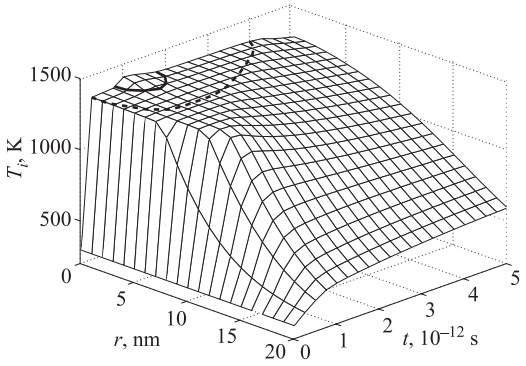

Fig. 2. $T_i(r,t)$ distribution for ion ^{129}Xe at 2.6 MeV/amu in $YBa_2Cu_3O_{7-x}$. The outer dotted line corresponds to $T_i = T_m$, the inner solid one marks the upper boundary between totally and partly molten phases at $T_i = T_m + \Delta$

The nonanalytical character of this function becomes apparent as a «plateau» designating the so-called mushy region near $T_i = T_m$. Resolutions to the phase transition problem of this type were found independently in different contexts in [35–37].

The numerical experiments have also revealed a threshold phenomenon taking place in the case when values of D_e and Q_f are big enough for a given magnitude of D_i. This sort of event is illustrated in Fig. 3, where temperatures of electrons along spatial trajectories, $r(t)$, of constant atom temperatures $T_i(r,t) = T_m + \Delta$, $T_i(r,t) = T_m$ and $T_i(r,t) = T_m - \Delta$ (curves a, b and c, accordingly) are depicted.

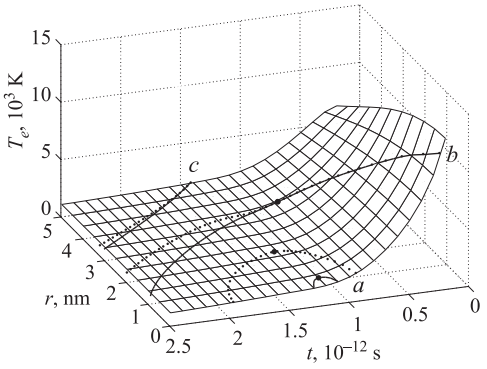

Fig. 3. Bifurcations of trajectories describing electron temperature along spatial points of constant atom temperatures $T_i(r,t) = T_m + \Delta$, $T_i(r,t) = T_m$ and $T_i(r,t) = T_m - \Delta$ (curves a, b and c, correspondingly) in $YBa_2Cu_3O_{7-x}$ for ^{129}Xe at 41 MeV/amu. Bold points belonging to lines a and b describe the maximal forward advance of the melting front, and, thus, for curves a they correspond to theoretical track radii. Dotted curve — $D_e = 0.222$; solid curve — $D_e = 0.223$

It is seen that the evolution of electron temperature along trajectories c and b undergoes a *bifurcation*, caused by slight variations of D_e. At the same time, this small modification of D_e leads to a sudden change of the a trajectory describing track formation in Fig. 3.

A reason for such irregular behavior is clarified in Figs. 4 and 5 where distributions of electron and lattice temperatures nearby a moment t_a corresponding to the time when the melting region radius mounts to its upper bound, $r = a$, are shown. «Plateaus» at $T_i = T_m$ in the figures testify to creation of molten phase due to electron heating. However, by the time t_a electron temperature within the track can become lower than T_m, so that the *«electronic quenching»* of the material got started (see Fig. 4). The opposite process, when atoms are still heated by electrons at moment t_a, possible under different experimental conditions is depicted in Fig. 5. Numerical experiments have shown that just transition from electronic heating to electronic quenching caused by small changes of D_e calls forth the instability shown in Fig. 3.

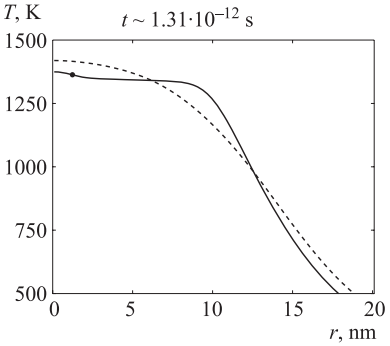

Fig. 4. $T_e(r)$ (dashed curve) and $T_i(r)$ (solid curve) distribution for ion ^{208}Pb at 3.7 MeV/amu in $YBa_2Cu_3O_{7-x}$. Point on solid curve denotes theoretical radius of track

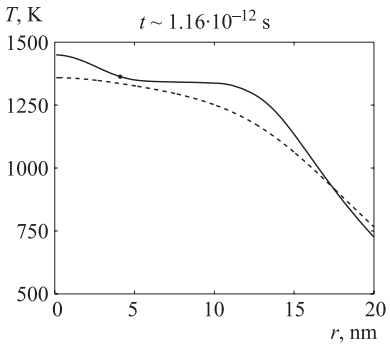

Fig. 5. $T_e(r)$ (dashed curve) and $T_i(r)$ (solid curve) distribution for ion ^{129}Xe at 10 MeV/amu in $YBa_2Cu_3O_{7-x}$. Theoretical radius of track is shown as a point on solid curve

Our calculations reveal that electronic quenching in $YBa_2Cu_3O_{7-x}$ always happens as soon as track formation time t_a exceeds $t_q = 1.24 \cdot 10^{-12}$ s.

6. DESCRIPTION OF TRACK RADII

A comparison of the length of time, τ_m, when the central region of the track and its boundary are retained at the temperature above the melting point can be estimated using two lower curves in Fig. 6. The influence of electronic quenching on the cooling rate is evident from comparison with two upper curves corresponding to artificial removal of the return atom–electron heat transfer taking place at $T_e < T_i$. Figure 6 allows one to examine the «epitaxial regrowth» hypothesis according to which the outer part of the track does not become amorphous due to a *short duration* of τ_m [8]. One can see that these values for temperature threshold $T_m + \Delta$ are indeed rather different (see points a_i in Fig. 6), whereas the corresponding values of τ_m are very close to each other for both T_m and $T_i = T_m - \Delta$ (points b_i and c_i, correspondingly). In fact, from a brief examination of (7) it follows that heat of fusion is mainly absorbed in a small temperature interval $T_m - \sigma \leqslant T_i \leqslant T_m + \sigma$ near

$T_i = T_m$, so that it is reasonable to take for *all* regions of the track $\tau_m \simeq 0.4 \cdot 10^{-11}$ s (see point b_3). Thus, calculations make dubious the existence of «epitaxial regrowth» on account of a smallness of τ_m for outer regions of the track.

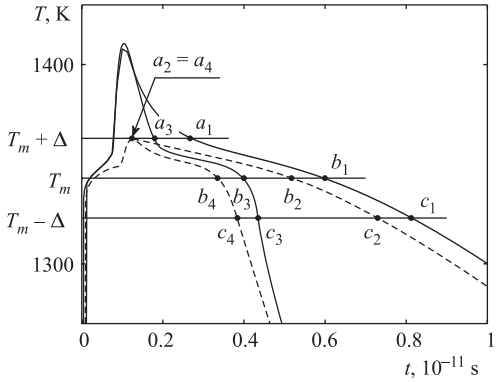

Fig. 6. Evolution of the lattice temperatures in the center of track and at its boundary (solid and dashed lines, accordingly) for the same ion as in Fig. 2

The cooling rate of the track is approximately equal to $dT_i/dt = 2.5 \cdot 10^{13}$ K/s the moment its temperature falls just below T_m. According to modern sound knowledge, it is more than enough to transfer the material into the amorphous state. For example, for creation of most metallic glasses cooling rates about $dT_i/dt \simeq 10^6$ K/s are sufficient, and for bulk materials $dT_i/dt = 10^3 \div 10$ K/s turns out to be quite enough [38]. Large cooling rate for $YBa_2Cu_3O_{7-x}$ refutes also the second possible reason for «epitaxial regrowth» assumed in [8].

Experimentally observed radii of tracks, $r_{\rm exp}$, in $YBa_2Cu_3O_{7-x}$ single crystal with [001] axis oriented parallel to the incident ion beam are given in table along with results of our calculations.

Experimentally observed radii of tracks, $r_{\rm exp}$, in $YBa_2Cu_3O_{7-x}$ single crystal taken from [39] and results of their theoretical description. Energy deposition dE/dx was calculated using [21]. Pseudodiffusivity of electrons, $D_e \equiv K_e/\rho C_e$, was taken to adjust the theoretical track radii to $r_{\rm exp}$. Uncertainties for ^{129}Xe at 41 MeV/amu are due to getting respective values into the bifurcation region (see Fig. 3)

Ion	E, MeV/amu	dE/dx, keV/nm	$r_{\rm exp}$, nm	a, nm	D_e, cm^2/s
^{129}Xe	1.3	26.2	2–3	2.71	0.730
^{129}Xe	2.6	30	2.5	2.49	0.768
^{129}Xe	10	27.9	1.3	1.35	0.605
^{129}Xe	27	18.7	1.3	1.6	0.326
^{129}Xe	41	14.8	0.56	0.44–1.55	0.223–0.222
^{208}Pb	3.7	43.7	4	4.1	1.130
^{208}Pb	10	42.5	3	3.02	1.015
^{208}Pb	20	37	3.5	3.52	0.805
^{208}Pb	25	34.5	3	3.06	0.732

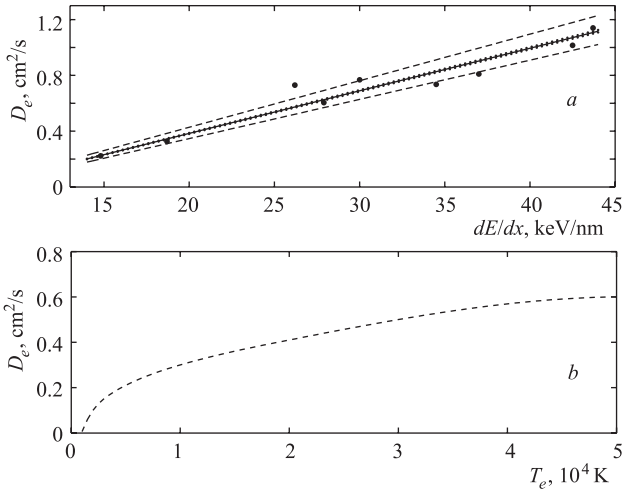

Fig. 7. *a*) Dependence of electron pseudodiffusivity D_e on energy deposition in $YBa_2Cu_3O_{7-x}$ found using the thermal spike model (points). Straight solid line describes the smoothed relationship, dashed lines demonstrate theoretical uncertainties resulting from experimental errors of parameter $\alpha = (1.3 \pm 0.1) \cdot 10^{-16}$ s/K. The role of the melting heat experimental errors is represented by small «waves» along the solid line. *b*) Theoretical $D_e(T_e)$ dependence for amorphous carbon extracted from [27]

Dependence of obtained electron pseudodiffusivity D_e on the energy deposition dE/dx is shown in Fig. 7, *a*. Main sources of errors, visible as point scattering around the solid line, are presumably fluctuation of experimental track radii [8] and inaccuracies of dE/dx. They should contribute to both vertical and horizontal jitter.

The figure gives a distinct evidence that parameter D_e for $YBa_2Cu_3O_{7-x}$ cannot be considered independent of the electron temperature, as is supposed in the Caen version of TSM. To speak in support of our conclusion, D_e as a function of T_e for amorphous carbon, calculated on the basis of theoretical results of [27], is shown in Fig. 7, *b*. It is seen that for this case pseudodiffusivity also increases essentially at electron temperatures $\sim 10^3$ K, which are typical for track formation in $YBa_2Cu_3O_{7-x}$ too (see Fig. 1). But what is more important is that the values of D_e established here turned out to be close indeed to the magnitude $D_e \simeq 1$ cm^2/s usually assumed in the Caen and some other track formation models. Therefore, we incline to consider the results of our theoretical estimations for this value to be realistic enough.

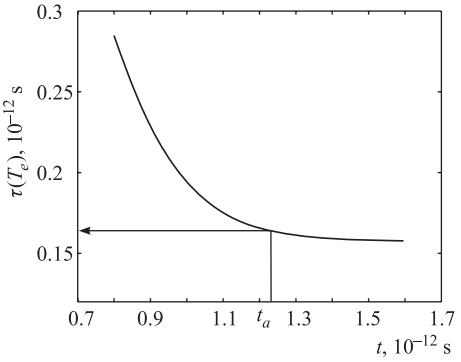

Fig. 8. $\tau(T_e(a,t))$ distribution for ion ^{129}Xe at 2.6 MeV/amu in $YBa_2Cu_3O_{7-x}$

Comparison of the theoretical electron–atom relaxation time with results of femtosecond laser experiments [15, 16] is not as trivial as it may appear. The time of molten region formation, t_a, defined in the previous section should not be confused with the time of electron–

atom relaxation, τ, although in the femtosecond laser experiments, where electrons get cold mainly due to local electron–atom interactions, they are in close agreement. However, the very existence of electron quenching signifies that primary electron cooling mode here is the electron thermal conductivity. Calculations have shown that in the case under consideration, due to influence of cold electrons at the boundary, the inequality $t_a \gg \tau$ takes place at the moment $t = t_a$. This is distinctly seen in Fig. 8 where $\tau(T_e)$ at the moving boundary of molten region is shown depending on time.

On the other hand, the value of $\tau(T_e)$ at the moment of track formation is always of the same order as that approximately determined in femtosecond laser experiments [15, 16].

CONCLUSIONS

The first assumptions that track formation in high-T_c superconductors can be described in the thermal spike framework were based on comparative analysis of tracks in different materials [8, 10]. These models were enough and did not give any evidence that such a description is not contradictory at least for one individual superconductor. The second step was an explanation of track constitution in $YBa_2Cu_3O_{7-x}$ that used much more detailed information concerning the concrete material [11]. It was elaborated closely to the Caen version of the TSM containing the free parameter $\lambda = \sqrt{D_e\tau}$. Besides, it utilized some fixed value of the electron diffusivity D_e, which magnitude is known, in fact, from some theoretical considerations only approximately, $D_e \simeq 1$ cm^2/s [14]. These uncertainties reduce noticeably significance of a conclusion of this paper that the mechanism responsible for track formation in high-T_c superconductor $YBa_2Cu_3O_{7-x}$ is the thermal spike one. In contrast to [11], the value of D_e has been *found* here to be approximately equal to 1 cm^2/s from the requirement the model has to describe experimental track radii, and at the same time *no free parameters* have been used. Therefore, calculations of D_e carried out on the basis of the thermal spike model look now very convincing. At the same time, very high sensitivity of track radii to a small change of D_e requires a special investigation.

The work is partially supported by the Russian Foundation for Basic Research, project No. 02-01-00606.

REFERENCES

1. *Konczykowski M. et al.* // Phys. Rev. B. 1991. V. 44. P. 7167.
2. *Hardy V. et al.* // Nucl. Instr. Meth. B. 1991. V. 54. P. 472.
3. *Civale L. et al.* // Phys. Rev. Lett. 1991. V. 67. P. 648.
4. *Lifshits I. M., Kaganov M. I., Tanatarov L. V.* // J. Nucl. Energy A. 1960. V. 12. P. 69.
5. *Fleischer R. L., Price P. B., Walker R. M.* Nuclear Tracks in Solids. Berkeley: University of California Press, 1979.
6. *Dartyge E.* // Phys. Rev. B. 1985. V. 32. P. 5429.
7. *Tanimura K., Itoh N.* // Phys. Rev. B. 1992. V. 46. P. 14362.

8. *Yimei Zhu et al.* // Phys. Rev. B. 1993. V. 48. P. 6436.

9. *Yimei Zhu, Cai Z. X., Welch D. O.* // Phil. Mag. A. 1996. V. 73. P. 1.

10. *Szenes G.* // Phys. Rev. B. 1996. V. 54. P. 12458.

11. *Goncharov I. N., Kostenko B. F., Philinova V. P.* // Phys. Lett. A. 2001. V. 288. P. 111.

12. *Toulemonde M., Dufour C., Paumier E.* // Phys. Rev. B. 1992. V. 46. P. 14362.

13. *Chadderton L. T., Torrens I. M.* Fission Damage in Crystals. London: Methuen, 1969.

14. *Meftah A. et al.* // Phys. Rev. B. 1994. V. 49. P. 12457.

15. *Brorson S. D. et al.* // Solid State Commun. 1990. V. 74. P. 1305.

16. *Vengrus I. I. et al.* // Pis'ma ZhETF. 1995. V. 62. P. 739.

17. *Allen P. P. et al.* // Phys. Rev. B. 1994. V. 49. P. 9073.

18. *Waligorski M. P. R., Hamm R. N., Katz R.* // Nucl. Tracks Radiat. Meas. 1986. V. 1. P. 309.

19. *Barashenkov V. S.* // Rus. Chem. High Energies. 1994. V. 28. P. 229.

20. *Meftah A. et al.* // Phys. Rev. B. 1993. V. 48. P. 920.

21. *Ziegler J. F.* SRIM 2003. Version 2003.26. www.srim org

22. *Ayrjan E. A., Fedorov A. V., Kostenko B. F.* // Part. Nucl., Lett. 2000. No. 2(99). P. 42.

23. *Krakauer H., Pickett W. E., Cohen R. E.* // J. Supercond. 1998. V. 1. P. 111.

24. *Crommil M. F., Zettle A.* // Phys. Rev. B. 1990. V. 41. P. 10978.

25. *Cohn J. L. et al.* Physical Properties of High Temperature Superconductors III / Ed. by D. M. Ginsberg. Singapore: World Scientific, 1992.

26. *Martynenko Yu. V., Yavlinski Yu. N.* // Sov. Fiz. Dokl. 1983. V. 28. P. 391; Preprint IAE-4084/11. M., 1985.

27. *Sciwietz G. et al.* // Nucl. Instr. Meth. B. 2000. V. 164–165. P. 354.

28. *Lusternik V. E. et al.* // Rus. Supercond.: Phys., Chem., Eng. 1990. V. 3. P. 2037.

29. *Teichler H.* // Phys. Rev. B. 1999. V. 59. P. 8473.

30. *Mironova G. M.* // Material Sci. Forum. 1993. V. 133–136. P. 847.

31. *Salama K., Lee D. F.* // Supercond. Sci. Technol. 1994. V. 7. P. 177.

32. *Idemoto Y., Fueki K.* // Jpn. J. Appl. Phys. 1990. V. 29. P. 2729.

33. *Wermbter S., Tewordt L.* // Physica C. 1991. V. 183. P. 365.

34. *Peaur S. D., Cohn J. L., Uher C.* // Phys. Rev. B. 1991. V. 43. P. 8721.

35. *Atthey D. R.* // J. Inst. Maths. Applics. 1974. V. 13. P. 53.

36. *Meirmanov A. M.* The Stefan Problem. Berlin; N. Y.: Walter de Gruyter, 1992.

37. *Kostenko B. F., Pribis J., Puzynin I. V.* math-ph/0302044; J. Comput. Meth. Sci. Eng. (to be published).

38. *Faupel F. et al.* // Rev. Mod. Phys. 2003. V. 75. P. 237.

39. *Toulemonde M., Bouffard S., Studer E.* // Nucl. Instr. Meth. B. 1994. V. 91. P. 108.

40. *Samarskii A. A.* Difference Schemes Theory. M.: Nauka, 1983.

41. *Kostenko B.F., Pribish J.* Mathematical modeling of track formation in high temperature superconductors / Bulletin of Peoples' Friendship University of Russia. Ser. «Applied and Computer Mathematics». 2005. V. 4, No. 1. P. 75.

Received on May 18, 2005.